International Journal on Magnetic Particle Imaging
Vol 10, No 1, Suppl 1, Article ID 2403008, 4 Pages

Infinite Science Publishing

Proceedings Article

Fourier neural operator for coupled Brown-Néel rotation model

Muhammed Hasan Kayapinar[a,*] · Asli Alpman[a,b,c] · Emine Ulku Saritas[a,b]

[a]Department of Electrical and Electronics Engineering, Bilkent University, Ankara, Turkey
[b]National Magnetic Resonance Research Center (UMRAM), Bilkent University, Ankara, Turkey
[c]Department of Electrical Engineering and Computer Sciences, University of California Berkeley, CA, USA
[*]Corresponding author, email: hasan.kayapinar@bilkent.edu.tr

Abstract

Modelling magnetization dynamics of magnetic nanoparticles (MNPs) is crucial to understand and predict their signal response in magnetic particle imaging (MPI). Coupled Brown-Néel rotation model expresses MNP magnetization as a system of ordinary differential equations (ODEs). However, numerical solution of these ODEs can be computationally intensive and time consuming using classical solvers. In this work, we propose a neural solver that utilizes a Fourier Neural Operator (FNO) to speed up the computation time for the coupled Brown-Néel rotation model. We show that the FNO model provides high signal fidelity with 5 orders of magnitude acceleration in computation time.

I. Introduction

Magnetic nanoparticles (MNPs) used in magnetic particle imaging (MPI) align with the externally applied magnetic field via two different relaxation processes: Brown rotation and Néel rotation. In the Brownian process, MNPs physically rotate to align their magnetic moments with the applied field, whereas in the Néel process, the magnetic moments internally rotate to align with the field [1]. These rotations occur simultaneously in a coupled fashion.

It is crucial to accurately model the magnetization dynamics of MNPs to have a better understanding of their behavior under different environmental settings. A previous study presented mathematical modeling of the coupled Brown-Néel rotation, expressing it as a system of ordinary differential equations (ODEs) [2]. This coupled model can be used for predicting the response of MNPs in different environmental settings, which can help determine the optimal operating settings for viscosity mapping and temperature mapping applications of MPI [3–5]. For this coupled model, numerical solutions of the ODEs for different sets of MNP parameters were previously utilized for MNP signal prediction via a model-based dictionary approach [6]. However, numerical solution of these ODEs are computationally intensive and time consuming.

A recent study showed that the non-coupled, Néel rotation based Fokker-Planck equation can be solved by using Fourier Neural operators (FNOs) to speed up the computation time [7]. Here, we propose a FNO model for the coupled Brown-Néel rotation model for an extensive set of MNP and environmental parameters. We demonstrate that when compared to a standard variable-step variable-order (VSVO) solver, the FNO model provides over 5 orders of magnitude reduction in computation time, while maintaining high fidelity solutions.

II. Methods and Materials

II.I. Fourier Neural Operator

Unlike other neural network architectures, where mapping is addressed between finite Euclidean spaces, the FNO performs a mapping between function spaces [8]. In other words, FNO enables the characterization of the mathematical model, instead of a direct input output relation. Hence, if the mapped function spaces are sampled densely enough, the FNO can encapsulate the natural interaction between function spaces [9]. As shown in Fig. 1a, there are multiple Fourier layers in the full network architecture, placed sequentially. Each Fourier layer combines properties of time- and frequency-domain features. As shown in Fig. 1b, in the first branch of the Fourier layer, a discrete time fast Fourier transform (FFT) of the input is taken. Then, a frequency-domain low pass filter is applied by R for harmonic selection and linear transformation. The cut-off frequency of the applied filter (k_{max}) is a hyper-parameter of the FNO model, and is chosen as 20 to process the first 20 harmonics. The result is converted to time domain by inverse FFT. The second branch of the Fourier layer performs a linear transformation, W, in time domain. The outputs of the two branches are then added and passed through a non-linear activation function, h. In our architecture, we utilized $L = 6$ Fourier layers.

II.II. Parameter Space Construction

In this work, we assumed a 1D drive field along the z-direction, as in the case of a magnetic particle spectrometer (MPS) setup. Selection fields or focus fields of an MPI scanner were not incorporated. We considered nine of the parameters ($N_p = 9$) within the coupled Brown-Néel rotation model. Our parameter space includes both explicit and implicit parameters. The applied field (B_i) and time values of the applied field (t) are implicit parameters. On the other hand, viscosity (η), amplitude (B_p) and frequency (f) of the applied drive field (DF), temperature (T), uniaxial magnetic anisotropy constant (K), particle core diameter (d_c), and hydrodynamic particle diameter (d_h) are the explicit parameters. We assumed that each parameter had a uniform distribution with a certain range and a certain step size, as listed in Table 1. The intervals were chosen to be as comprehensive as possible to construct a model that works for a wide set of parameters. Saturation magnetization and Gilbert damping constant were kept constant at 360 kA/m and 0.1 respectively.

Each of the training samples was assumed to be drawn in an independent and identically distributed (i.i.d.) fashion. The total number of training samples was N=10,000 (i.e., 10,000 different combinations of the 7 parameters listed in Table 1), whereas the validation and test sets contained 1000 samples each. Each $B_i \in \mathbb{R}^{N_t \times 1}$ contained $N_t = 200$ time points per period of the DF (where i = 1,2 ... N). Each sample from sample space was stored in a matrix a_i, where columns represented both implicit and explicit parameters. For the 7 explicit parameters that were kept constant through time, we generated vectors of size $\mathbf{1}_{N_t \times 1}$. Then, we multiplied with the corresponding parameter values before placing these vectors into the matrix $a_i \in \mathbb{R}^{N_t \times N_p}$.

Table 1: Explicit parameters of the parameter space. Each parameter was assumed to be drawn from a uniform distribution of range and step size given in the table.

Parameter	Range	Step Size
B_p	$(5, 25)$ mT	1 mT
f	$(250, 10000)$ Hz	1 Hz
K	$(0, 10000)$ J/m^3	1 J/m^3
T	$(25, 45)$ °C	1 °C
d_c	$(10, 30)$ nm	1 nm
d_h	$(25, 130)$ nm	1 nm
η	$(0.89, 15.33)$ mPa.s	0.01 mPa.s

II.III. Problem Formulation

The network was trained using an ℓ_2 loss defined as

$$L(y, \hat{y}) = \frac{\|y - \hat{y}\|_2^2}{\|y\|_2^2}$$

where $y \in \mathbb{R}^{N_t \times 1}$ represents the ground-truth signal vector obtained from VSVO solver and $\hat{y} \in \mathbb{R}^{N_t \times 1}$ represents the signal vector predicted by the network. Adam optimizer was used with a weight decay coefficient of 10^{-4} to prevent over-fitting. A learning rate scheduler was utilized for robust learning. The associated hyperparameters were step size = 150, $\gamma = 0.5$, and learning rate $\alpha =$ 0.001. When the epoch count reached multiples of the step size, the learning rate was updated as $\gamma \cdot \alpha$. Reducing the learning rate helped resolve the finer details in the predicted signal. The number of epochs was set to 1500.

Normally, the output of the coupled Brown-Néel rotation ODEs is the magnetic moment of the MNP. However, we applied a direct mapping to its time derivative to directly access the MNP signal. We also divided each signal with the applied field amplitude and frequency for signal normalization. This normalization step restricts the amplitude of the predicted signal to a narrower range, facilitating the training of the network. Each signal vector was stored in $y_i \in \mathbb{R}^{N_t \times 1}$. Hence, our training pair was (a_i, y_i) where i=1,2, ..., N.

10.18416/ijmpi.2024.2403008

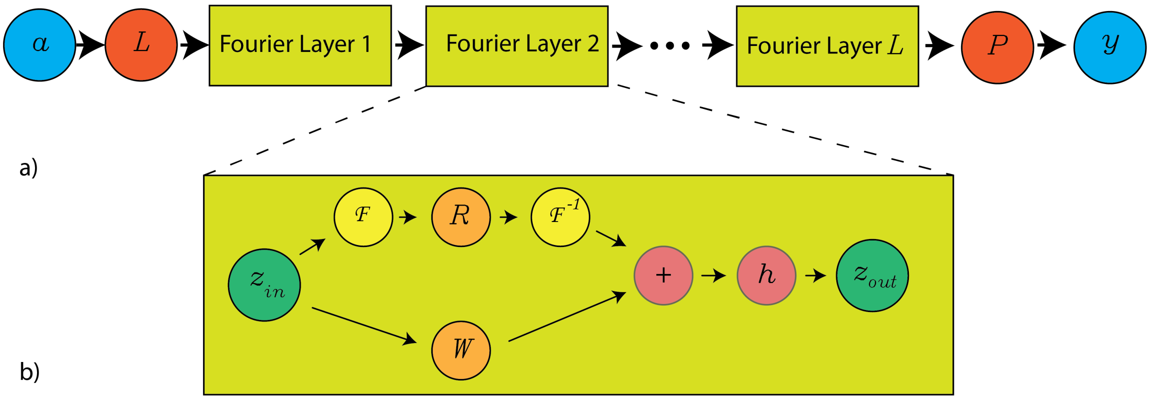

Figure 1: Architecture of the FNO. (a) The overall network architecture incorporates multiple, sequentially placed Fourier layers. (b) Each Fourier layer combines time- and frequency-domain features. L and P represent the fully connected layers. a is lifted to higher dimension and projected onto the lower dimension by these layers, respectively. R represents the frequency domain low pass filter, W denotes linear transformation, and h denotes the non-linear activation function.

Table 2: Computation time for the test samples for VSVO solver and FNO model, and NRMSE for FNO with respect to VSVO. Median (25^{th}-75^{th} percentile) values are listed.

Method	Computation Time (sec)	NRMSE (%)
VSVO	504.38 (240.28-737.12)	-
FNO	0.0026 (0.0025-0.0027)	0.61 (0.36-1.30)

II.IV. Implementation Details

The VSVO solver was implemented using *ode15s* built-in function of MATLAB [10]. This implementation was performed on a CPU (Intel x86-64) due to the sequential nature of the algorithm. The FNO model was implemented in Python with the Pytorch deep learning framework. The training of the model was performed on a GPU (NVIDIA GeForce GTX 1050 Ti). To enable comparison of computation times, the inference for the FNO model was performed on the same CPU as the VSVO solver.

For quantitative assessments, we used the normalized root mean square error (NRMSE) defined as:

$$\mathrm{NRMSE} = \frac{\|y-\hat{y}\|_2}{\sqrt{N_t}(\max(y)-\min(y))}$$

III. Results and Discussion

Figure 2 shows four representative results from the test set, comparing the signal predicted by the FNO model with the ground-truth signal from VSVO solver. These results demonstrate that the FNO model successfully captures the subtle variations in the MNP signals for a wide range of parameters. For these 4 cases, the mean computation times were 419.54 sec and 0.0027 sec for VSVO solver and FNO model, respectively. The mean NRMSE of signals predicted by the FNO was 0.26%, when compared to the ground-truth signals.

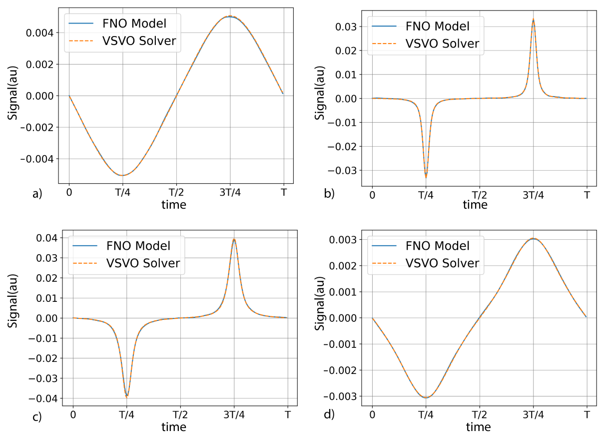

Figure 2: Four representative results for the FNO model, compared with the ground-truth signals from VSVO solver. (a) Results for f=588 Hz, B_p=7 mT, K=4855 J/m^3, T=26 °C, η=9.67 mPa.s, d_c=14 nm, d_h=41 nm. (b) Results for f=2931 Hz, B_p=24 mT, K=60 J/m^3, T=39 °C, η=6.46 mPa.s, d_c=27 nm, d_h=100 nm. (c) Results for f=5475 Hz, B_p=11 mT, K=1735 J/m^3, T=43 °C, η=2.06 mPa.s, d_c=26 nm, d_h=55 nm. (d) Results for f=6492 Hz, B_p=23 mT, K=5168 J/m^3, T=37 °C, η=15.33 mPa.s, d_c=12 nm, d_h=52 nm.

As listed in Table 2, the median computation timesacross all 1000 test samples were 504.38 sec and 0.0026 sec for the VSVO solver and the FNO model, respectively. The total computation time for all 1000 test samples was approximately 6 days for the VSVO solver, in contrast to 2.64 sec for the FNO model. The NRMSE of the predicted signals have a median (25^{th}-75^{th} percentile) of 0.61% (0.36%-1.30%). Hence, our FNO model is approximately 195,000 times faster than the VSVO solver, while maintaining high signal fidelity.

10.18416/ijmpi.2024.2403008

It should be mentioned that while the NRMSE values remain quite small for the majority of the cases, there were a few outlier cases for which the NRMSE reached 21%. Most notably, these outlier cases had large core diameters. Potential parameters to investigate here are the number of harmonics included during the harmonic selection, and the number of time points in a period. Further analysis of these outlier cases and investigation of potential solutions remains a topic of future work.

IV. Conclusion

In this work, we proposed a FNO model for the coupled Brown-Néel rotation model, and demonstrated its performance for an extensive set of MNP parameters and environmental parameters. The results show that the FNO model provides a significant advantage in computation time with near exact prediction of the MNP signal from a VSVO solver. This reduction in computation time can enable analysis of MNP behaviour under a wide range of settings for applications, such as determining the optimal DF settings for viscosity mapping or temperature mapping.

Acknowledgments

This work was supported by the Scientific and Technological Research Council of Turkey (TUBITAK 120E208).

Author's statement

Conflict of interest: Authors state no conflict of interest.

References

[1] C. Shasha and K. Krishnan. Nonequilibrium dynamics of magnetic nanoparticles with applications in biomedicine. *Advance Materials*, 33(23):1904131, 2020, doi:10.1002/adma.201904131.

[2] J. Weizenecker. The fokker–planck equation for coupled brown–néel-rotation. *Physics in Medicine & Biology*, 63(3):035004, 2018, doi:10.1088/1361-6560/aaa186.

[3] C. Stehning, B. Gleich, and J. Rahmer. Simultaneous magnetic particle imaging (mpi) and temperature mapping using multi-color mpi. *International Journal on Magnetic Particle Imaging*, 2(2):612001, 2016, doi:10.18416/ijmpi.2016.1612001.

[4] M. Möddel, C. Meins, J. Dieckhoff, and T. Knopp. Viscosity quantification using multi-contrast magnetic particle imaging. *New Journal of Physics*, 20:083001, 2018, doi:10.1088/1367-2630/aad44b.

[5] M. Utkur and E. U. Saritas. Simultaneous temperature and viscosity estimation capability via magnetic nanoparticle relaxation. *Medical Physics*, 49(4):2590–2601, 2022, doi:10.1002/mp.15509.

[6] A. Alpman, M. Utkur, and E. U. Saritas. Mnp characterization and signal prediction using a model-based dictionary. *International Journal on Magnetic Particle Imaging*, 8(1):203017, 2022, doi:https://doi.org/10.18416/IJMPI.2022.2203017.

[7] T. Knopp, H. Albers, M. Grosser, M. Möddel, and T. Kluth. Exploiting the fourier neural operator for faster magnetization model evaluations based on the fokker-planck equation. *International Journal on Magnetic Particle Imaging*, 9(1):303003, 2023, doi:https://doi.org/10.18416/IJMPI.2023.2303003.

[8] Z. Li, N. Kovachki, K. Azizzadenesheli, B. Liu, K. Bhattacharya, A. Stuart, and A. Anandkumar. Fourier neural operator for parametric partial differential equations, 2021. arXiv: 2010.08895 [cs.LG].

[9] N. B. Kovachki, Z. Li, B. Liu, K. Azizzadenesheli, K. Bhattacharya, A. M. Stuart, and A. Anandkumar. Neural operator: Learning maps between function spaces. *CoRR*, abs/2108.08481, 2021. arXiv: 2108.08481. URL: https://arxiv.org/abs/2108.08481.

[10] L. F. Shampine and M. W. Reichelt. The matlab ode suite. *SIAM Journal on Scientific Computing*, 18(1):1–22, 1997, doi:10.1137/S1064827594276424.

